High resolution wavefront correction with photocontrolled deformable mirror

S. Bonora,[1*] D. Coburn,[2] U. Bortolozzo,[3] C. Dainty,[2] and S. Residori[3]

[1]*CNR-IFN, Laboratory for Ultraviolet and X-ray Optical Research, via Trasea 7, 35131 Padova, Italy*
[2]*National University of Ireland, Department of Physics, Applied Optics group, Galway, Ireland*
[3]*INLN, Universite´ de Nice Sophia Antipolis, CNRS; 1361 route des Lucioles, 06560 Valbonne, France*
[*]*stefano.bonora@dei.unipd.it*

Abstract: We demonstrate that a novel actuation scheme, employed in an optical control deformable mirror, can be more convenient than the conventional discrete fixed actuators approach. The Photo-Controlled Deformable Mirror (PCDM) mirror leverages consumer LCD display technology in the wavefront forming control, enabling flexible programmable configuration of the actuation geometry. This new approach simplifies the driving electronics, relaxing the per channel cost of high spatial control of the wavefront forming surface. In our experiment we tested the PCDM by applying the equivalent of 36, 76 and 201 actuators, this by just changing the light driving pattern. We demonstrated the effectiveness of this technique in a closed loop setup, which showed performances superior to the state of the art for similar DM, while providing a significant reduction in the hardware complexity.

OCIS codes: (010.1080) Active or adaptive optics; (230.2090) Electro-optical devices.

References and links

1. J. W. Hardy, *Adaptive Optics for Astronomical Telescopes* (Oxford Series in Optical and Imaging Sciences, 1998).
2. A. Dubra and Y. Sulai, "Reflective afocal broadband adaptive optics scanning ophthalmoscope," Biomed. Opt. Express **2**(6), 1757–1768 (2011).
3. E. A. Rossi, M. Chung, A. Dubra, J. J. Hunter, W. H. Merigan, and D. R. Williams, "Imaging retinal mosaics in the living eye," Eye (Lond.) **25**(3), 301–308 (2011).
4. J. Carroll, A. M. Dubis, P. Godara, A. Dubra, and K. E. Stepien, "Clinical applications of retinal imaging with adaptive optics," US Ophthalmic Review **4**, 78–83 (2011).
5. R. Tyson, *Adaptive Optics Engineering Handbook* (Optical Science and Engineering 2005).
6. M. Rueckel, J. A. Mack-Bucher, and W. Denk, "Adaptive wavefront correction in two-photon microscopy using coherence-gated wavefront sensing," Proc. Natl. Acad. Sci. U.S.A. **103**(46), 17137–17142 (2006).
7. C. Bonato, A. V. Sergienko, B. E. Saleh, S. Bonora, and P. Villoresi, "Even-order aberration cancellation in quantum interferometry," Phys. Rev. Lett. **101**(23), 233603 (2008).
8. H. C. Kapteyn, R. Bartels, S. Backus, E. Zeek, L. Misoguti, G. Vdovin, I. P. Christov, and M. M. Murnane, "Shaped-pulse optimization of coherent emission of high-harmonic soft X-rays," Nature **406**(6792), 164–166 (2000).
9. S. Bonora, D. Brida, P. Villoresi, and G. Cerullo, "Ultrabroadband pulse shaping with a push-pull deformable mirror," Opt. Express **18**(22), 23147–23152 (2010).
10. D. Brida, C. Manzoni, G. Cirmi, M. Marangoni, S. Bonora, P. Villoresi, S. De Silvestri, and G. Cerullo, "Few-optical-cycle pulses tunable from the visible to the mid-infrared by optical parametric amplifiers," J. Opt. **12**(1), 013001 (2010).
11. P. Villoresi, S. Bonora, M. Pascolini, L. Poletto, G. Tondello, C. Vozzi, M. Nisoli, G. Sansone, S. Stagira, and S. De Silvestri, "Optimization of high-order harmonic generation by adaptive control of a sub-10-fs pulse wave front," Opt. Lett. **29**(2), 207–209 (2004).
12. N. Devaney, E. Dalimier, T. Farrell, D. Coburn, R. Mackey, D. Mackey, F. Laurent, E. Daly, and C. Dainty, "Correction of ocular and atmospheric wavefronts: a comparison of the performance of various deformable mirrors," Appl. Opt. **47**(35), 6550–6562 (2008).
13. U. Bortolozzo, S. Bonora, J. P. Huignard, and S. Residori, "Continuous photocontrolled deformable membrane mirror," Appl. Phys. Lett. **96**(25), 251108 (2010).

#158841 - $15.00 USD Received 1 Dec 2011; revised 13 Feb 2012; accepted 13 Feb 2012; published 16 Feb 2012

14. S. Bonora, M. Meneghini, A. Marrani, M. Bassi, I. Falco, and E. Zanoni, "Photostrictive effect in a polyvinylidene fluoride-trifluoroethylene copolymer," Appl. Phys. Lett. **99**(3), 033506 (2011).
15. J. C. Chanteloup, H. Baldis, A. Migus, G. Mourou, B. Loiseaux, and J.-P. Huignard, "Nearly diffraction-limited laser focal spot obtained by use of an optically addressed light valve in an adaptive-optics loop," Opt. Lett. **23**(6), 475–477 (1998).
16. R. Ragazzoni, "Pupil plane wave front sensing with an oscillating prism," J. Mod. Opt. **43**(2), 289–293 (1996).
17. J. Farinato, V. Viotto, R. Ragazzoni, C. Arcidiacono, A. Baruffolo, M. Dima, G. Gentile, D. Magrin, and P. Rossettini, "A compact design of a WFS for a natural guide star based ELT adaptive optics system," Proc. SPIE **7736**, 77362M, 77362M-7 (2010).
18. R. Ragazzoni, C. Arcidiacono, M. Dima, J. Farinato, D. Magrin, and V. Viotto, "Adaptive optics with solely natural guide stars for an extremely large telescope," Adaptive Optics Systems II, Proc. of SPIE **7736**, 773623 (2010).
19. J. Khoury, A. Drehman, C. L. Woods, B. Haji-Saeed, S. K. Sengupta, W. Goodhue, and J. Kierstead, "Optically driven microelectromechanical-system deformable mirror under high-frequency AC bias," Opt. Lett. **31**(6), 808–810 (2006).
20. S. Bonora, I. Capraro, L. Poletto, M. Romanin, C. Trestino, and P. Villoresi, "Wave front active control by a digital-signal-processor-driven deformable membrane mirror," Rev. Sci. Instrum. **77**(9), 093102 (2006).
21. C. Paterson, I. Munro, and J. Dainty, "A low cost adaptive optics system using a membrane mirror," Opt. Express **6**(9), 175–185 (2000), http://www.opticsinfobase.org/oe/abstract.cfm?uri=oe-6-9-175.
22. S. Bonora and L. Poletto, "Push-pull membrane mirrors for adaptive optics," Opt. Express **14**(25), 11935–11944 (2006).
23. P. Aubourg, J. P. Huignard, M. Hareng, and R. A. Mullen, "Liquid crystal light valve using bulk monocrystalline $Bi_{12}SiO_{20}$ as the photoconductive material," Appl. Opt. **21**(20), 3706–3712 (1982).
24. L. Thibos, R. Applegate, J. Schwiegerling, R. Webb, and VSIA Standards Taskforce Members, "Standards for reporting the optical aberrations of the eye," in *Vision Science and its Applications*, OSA Technical Digest (Optical Society of America, 2000), paper SuC1.

1. Introduction

In the last decade many scientific fields have benefitted from the use of Adaptive Optics (AO) devices. Astronomy [1], ophthalmology [2–4], optical communications [5], microscopy [6], quantum engineering [7], coherent control [8, 9], femtosecond lasers for pulse compression [10, 11] are some of the fields where the introduction of a Deformable Mirror (DM) has been the key for improved performance. Since each application has specific requirements, several DM technologies and actuation methods are currently in use (e.g. voice coil actuation, electrostatic, piezo). Each of them gives a different balance among correction speed, system stability, stroke, resolution and aperture. Ref [12] compares the performance of the most popular DMs in 2008. Magneticly actuated DMs can generate high stroke, while Micro Electro Mechanical Systems (MEMS) DMs can achieve the highest spatial resolution. Recently, we introduced a novel technology where the wavefront control is based on optically addressable actuators realized via a photoconductive substrate [13, 14]. While the association of a photoconductor with liquid crystals is consolidated [15], its association with deformable surfaces is new. Such a photo-controlled deformable mirror, (PCDM) is driven by the light intensity distribution that is projected on its back side, where the photosensitive layer is placed. Compared to other deformable mirrors, the PCDM does not have fixed electrode channels for actuation, nor does it require a dedicated high voltage amplifier per actuator site. The main advantages, when compared with the other standard technologies, are: the reduction of the hardware complexity, high spatial resolution in wavefront forming ability and the promise of compactness for high actuator densities together with the reconfigurability of any actuator pattern.

Because of its features, the PCDM appears to be promising for the realization of high spatial density wavefront actuation. It is also appealing for the realization of large size deformable mirrors with many actuators, as are required, for instance, for extreme astronomy applications where high resolution wavefront sensors are already a well-established technology [16]. High spatial density state-of-the-art DMs have been realized by using tens of thousands of discrete PZT or MEMS actuation channels. However, the per channel cost and the difficulties related to the fabrication procedure, coupled with the cost of the driving electronics (such as high voltage amplifiers and control unit), make them quite expensive and,

#158841 - $15.00 USD Received 1 Dec 2011; revised 13 Feb 2012; accepted 13 Feb 2012; published 16 Feb 2012

hence, not appealing for widespread applications. A larger version of the device presented in this paper, coupled with a high resolution wavefront sensor, has been envisaged by the astronomy community for its use with large telescopes [17, 18]. Moreover the PCDM meets some important industrial and manufacturing issues. In fact, the reduced reliance on multiple independent drive channels offers clear promise in terms of the robustness of the device to failure for a consumer device since the lifetimes of the underlying projection technology is superior to DMs using multichannel systems with high voltage.

Although a few prototypes of PCDM have already been reported in literature [13, 19], their capability in terms of high spatial resolution and their use in an adaptive optics setup have not been explored yet. The aim of this paper is to demonstrate the PCDM capability in providing high performance adaptive optics implementations. To this end, we have employed the PCDM in a closed loop adaptive optics system and tested its flexibility and ease of use through the generation of Zernike polynomials surface deformations. Moreover, high spatial resolution addressing has been realized and demonstrated. The results here presented allow for a straightforward comparison with other DMs characterized by a similar aperture or a similar technology.

2. Description of the PCDM

The PCDM is an electrostatic membrane deformable mirror [20, 21], where the electrode pads, used conventionally in membrane mirror devices, have been replaced by a photoconductive crystal [13, 15]. Among available photoconductors (for instance, Silicon or Gallium Arsenide [19]), we have used a Bismuth Silicon Oxide (BSO) crystal because it has the advantage of presenting a low absorption coefficient, which allows a large penetration depth, and of being characterized by a capacitance similar to the one formed by the membrane, thus, allowing for a large modulation of the voltage drop across the membrane mirror.

The PCDM is driven by a Liquid Crystal Display (LCD) 800x 600pixels (active area = 9mm x 12mm), which is illuminated with a high power blue Light Emitting Diode (LED). As illustrated in Fig. 1, the LCD is imaged on the back of the PCDM by the use of a lens and is aligned to the center of the BSO. The projected beam size is 11mm x 11mm, which sets the extent of the active region.

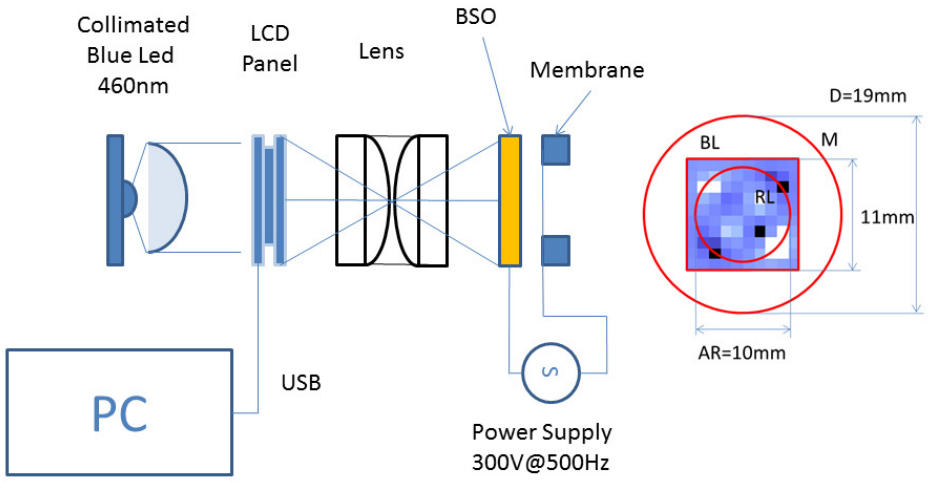

Fig. 1. Right hand side: PCDM drive optics. Left hand side: PCDM control pixel geometry mapped to the BSO crystal for a 10 x 10 configuration. BL Blue Light from the LCD driving display showing an example of 10x10 actuators pattern, M Membrane border, AR active region.

#158841 - $15.00 USD Received 1 Dec 2011; revised 13 Feb 2012; accepted 13 Feb 2012; published 16 Feb 2012

The LCD has a 12bit vertical resolution and is driven by the control computer via an HDMI port (addressed in the current system via a USB to HDMI adaptor). The controller allows for the 600 x 600 active pixels (those mapping to the active region of the BSO crystal) to be grouped into regular subsets of larger control pixels of more practical size for the AO controller. Three configurations were tested: 6x6, 10x10 and 15x15 control pixel grouping. The first case generates the equivalent of 36 actuators where each control maps a 100x100 subset of LCD pixels, while in the second case we had the equivalent of 76 actuators (10x10 equivalent arrangement where the electrodes outside a circular pupil were kept off) and in the third case the equivalent of 201 actuators (15x15 equivalent arrangement where the electrodes outside a circular pupil were kept off). Figure 1 shows the position of the blue driving light and of the active region with respect to the boundaries of the membrane and an example of blue pattern illumination with a subdivision into 10x10 actuators.

The DM membrane aperture is D = 19mm diameter. As suggested in literature [21, 22] the optimal value of the system aperture is of the order of 0.6 times the diameter of the whole membrane while there should be at least one ring of actuators outside it. The intensity of the blue light on the back of the photoconductor when the LCD was at its maximum transmission state was about 20mW/cm^2. The working parameters of the power supply were 165V@700Hz. These parameters were employed to optimize the PCDM stroke while at the same time minimizing the impact of the AC power supply oscillations on the measured results and system operation [13]. The time response of the PCDM is given by three factors: the mechanical response of the membrane, the time constant of the capacitive coupling, and the response of the LCD modulator. The LCD is designed to work at video rate of 25 frames per second. The rest of the system exhibits a measured rise time of about 17ms on the fundamental mode. The calibration of the stroke was validated by characterizing the wavefront peak to valley measured with the wavefront sensor as the blue LED light level was modulated by the LCD for a series of uniform control values. Figure 2 shows the sigmoidal modulation of the PCDM stroke as a function of the gray level on the LCD (response of system without linearization). In the AO controller this function is inverted by the mirror drive software, mapping the linear control update from the AO controller to the non-linear operating characteristic of the LCD modulation, in order to have a linear modulation as required by the closed loop system. Figure 2 shows both the nonlinear modulation of the LCD (left panel) and the linearized response in the right panel.

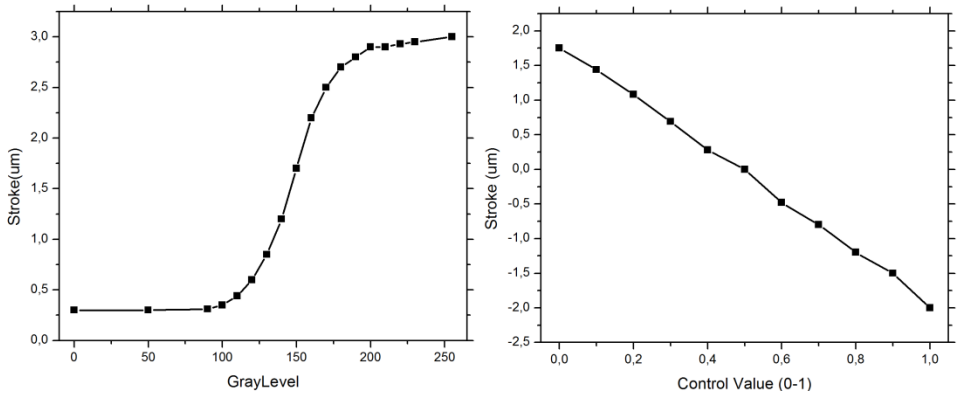

Fig. 2. , left panel: The measured DM stroke (PV) in function of the gray scale of the LCD panel. Right panel:Stroke of the PCDM linearized.

#158841 - $15.00 USD Received 1 Dec 2011; revised 13 Feb 2012; accepted 13 Feb 2012; published 16 Feb 2012

3. Equivalent electric model

The PCDM can be modeled with its electrical equivalent circuit, as shown in Fig. 3. A similar modeling was introduced for light-valves using the same BSO photoconductor but in association with liquid crystals [23].

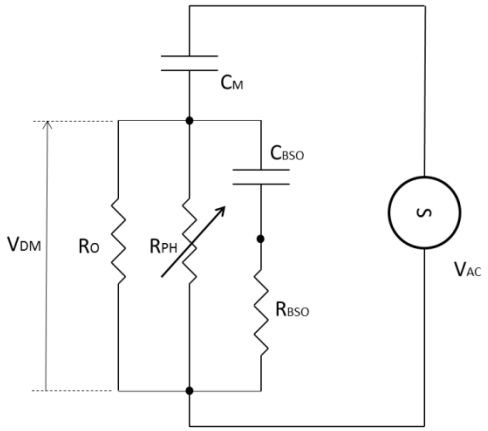

Fig. 3. Equivalent electrical model of the PCDM.

The membrane forms a capacitor C_M while the BSO crystal is modeled as a parallel between the BSO dark resistor R_o, the photoconductor resistor R_{PH} and the series between a capacitor C_{BSO} and a resistor R_{BSO}.

The electrical elements have the following values:

$$C_{DM} = \frac{\varepsilon_0 A}{t_{DM}} = 50\,pF \tag{1}$$

$$C_{BSO} = \frac{\varepsilon_0 \varepsilon_{BSO} A}{t_{BSO}} = 56\,pF \tag{2}$$

$$R_O = \frac{t_{BSO}}{\sigma_{BSO} A} \tag{3}$$

where t_{DM} = 50μm is the distance photoconductor-membrane, $A = \pi(D/2)^2$ is the membrane surface 283mm^2, the BSO thickness t_{BSO} is 1 mm, the BSO dielectric constant is $\varepsilon_{BSO} = 56$ and its dark conductivity is σ_{BSO} is $10^{-12}\Omega^{-1}$ [20].

Than the resistor value R_{PH} is inversely proportional to the intensity according to [23]:

$$R_{PH} = \frac{t_{BSO}}{\sigma_{PH}(I) A} = \frac{t_{BSO}}{\alpha I \sigma_{BSO} A} \tag{4}$$

where I is the intensity on the photoconductor and α was estimated to be 138cm^2/W. The value of R_{BSO} has been estimated from the data to be: R_{BSO} = 20MΩ.

Then the voltage drop V_{DM} across the membrane can be calculated as:

$$V_{DM} = V_{AC} \left[\left(\frac{1}{j\omega C_M} + R_{BSO} \right)^{-1} + \frac{1}{R_0} + \frac{1}{R_{PH}(I)} \right]^{-1} \Bigg/ \left\{ \frac{1}{j\omega C_M} + \left[\left(\frac{1}{j\omega C_M} + R_{BSO} \right)^{-1} + \frac{1}{R_0} + \frac{1}{R_{PH}(I)} \right]^{-1} \right\} \tag{5}$$

#158841 - $15.00 USD Received 1 Dec 2011; revised 13 Feb 2012; accepted 13 Feb 2012; published 16 Feb 2012

From the model and the physical parameters of the system detailed earlier we obtained the results shown below in Fig. 4. The normalized electrostatic pressure on the membrane is plotted as a function of the blue light intensity for a number of different operating frequency of the voltage applied to the PCDM. Theoretical predictions compared with the corresponding experimental results indicated by the data points in the plot show an excellent agreement. The right panel of Fig. 4 shows that the PCDM modulates the electrostatic pressure proportionally to the light driving intensity [13]. The results show the amount of the power supply that can drop on the membrane. The fraction of voltage is zero for frequencies above 5kHz while it becomes bigger for lower frequencies. We set the working frequency to 700Hz which is just above the mechanical cut off response of the membrane to minimize unwanted membrane oscillations (otherwise detected by the system wavefront sensor) obtaining a stroke of about 10μm similar to the one typical of electrostatic membrane mirrors [20].

4. Experimental setup

The main goal of our work was to demonstrate the effectiveness of the PCDM in a closed loop adaptive optics setup. Primarily we wanted to perform a preliminary study on the performance of the mirror in a closed loop system for different actuator geometries, thus underline the flexibility of the system in this regards. In addition we also used the AO controller to characterize the performance of the mirror in the generation of Zernike polynomials. We set predefined offsets to the AO controller. The experimental setup for the closed-loop used to test the PCDM is illustrated if Fig. 5. The system is composed by a 630nm laser point source which is first collimated (*Arm 1*) before being directed through a beamsplitter and then expanded, through a x2 afocal lens assembly (*Arm 2*), to match the active area of the PCDM, which is of 10mm diameter region. In the third arm of the setup, the beam reflected by the PCDM enters a high resolution Shack-Hartmann wavefront sensor (WFS) via reflection on the beam splitter on its return path through the afocal pair. The WFS has an measurement aperture of 5mm (mapping as a 2:1 ratio to the active region of the mirror). In the test arrangement the phase plate, the PCDM and the WFS form conjugate planes of the optical system (A, B, C in Fig. 5).

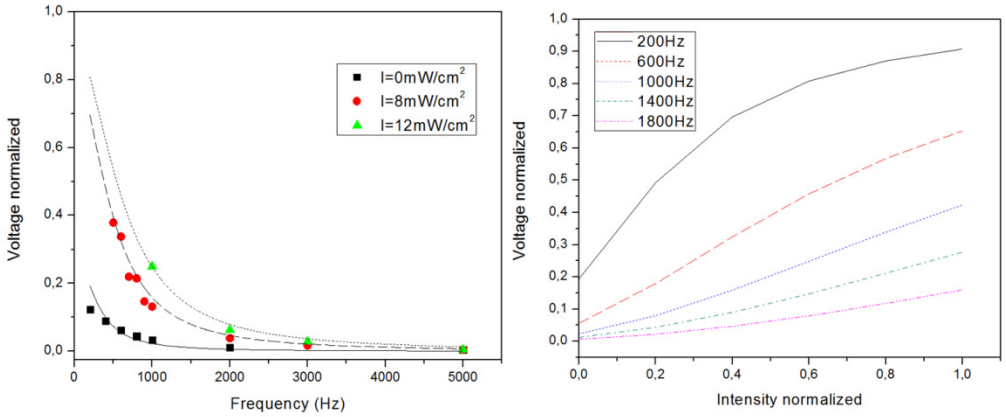

Fig. 4. Left panel, measurement (points) and simulations (dashed lines) of the normalized voltage drop on the membrane in function of the frequency of the power supply under uniform illumination at different intensities. Right panel: normalized voltage on the membrane in function of the driving light intensity.

We tested the closed loop system by first biasing the PCDM while setting the illumination on the photoconductor to its middle stoke level via the actuator control values. This was recorded with the wavefront sensor as the reference wavefront for the AO controller. Then we acquired the influence functions for the particular geometry by pushing and pulling on each

#158841 - $15.00 USD Received 1 Dec 2011; revised 13 Feb 2012; accepted 13 Feb 2012; published 16 Feb 2012

actuator site in turn one at a time via control of the actuator pixels (i.e. setting its color to black and white). Each virtual actuator is set to black and then white, while keeping all the others to the middle stoke level. The influence function is given by the average of the relative wavefront displacement. The AO controller employed a conventional integrator control scheme and ran at a control loop frame rate of 15.7Hz (dictated by the frame rate of the WFS for the particular configuration employed).

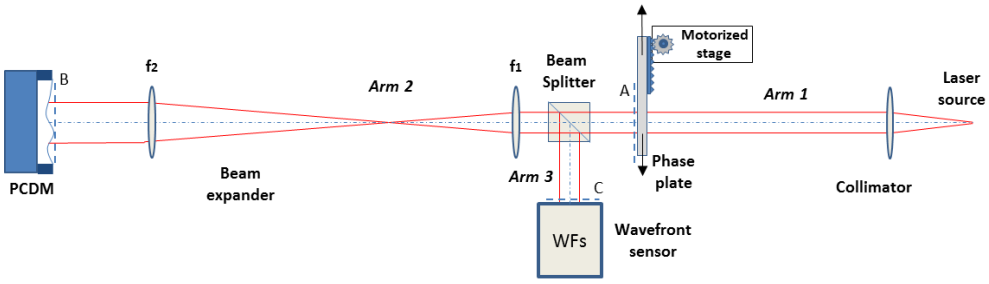

Fig. 5. Closed loop setup for the demonstration of the PCDM correction capabilities. The aberrations are generated by the phase plate placed in the plane A, which is conjugated with the plane B on the PCDM and C on the wavefront sensor. Arm 1: collimator and phase screen for time changing aberrations; Arm 2: afocal lens x 2 – 5mm to 10mm, f_1 = 100mm, f_2 = 200mm; Arm 3: Shack-Hartmann WFS, lenslet pitch 300µm, focal length 18mm.

The reconstructor matrix used in the AO control was calculated using a truncated SVD (Singular Value Decomposition) pseudo inverse based on the influence function data set. As usual, SVD truncation was employed to discard high order, noise sensitive mirror modes in order to improve the condition of the reconstructor, thus, stabilizing the controller against noise amplification (see [21]). In closed loop operation the reconstructor output was fed to the integrator to produce the linear control update for the mirror. This was achieved by mapping the non-linear operating characteristics of the LCD and by using the mapping function detailed earlier to produce a control grey scale to apply to the LCD in order to achieve the desired wavefront correction.

Initially, the AO correction performance of the system was tested by monitoring its response to time varying aberrations for differing electrode geometries. These were created by inserting a phase screen in the collimator, *Arm 1*, of the system, at a plane conjugate to the position of the PCDM and, in turn, to the WFS (planes A, B, C in Fig. 5). The phase screen was mounted on a motor drive stage that moves the phase screen at a peak rate of 0.45mm/s for 5mm forward and back along the path of the beam first with the AO loop off and then repeated with the AO loop on. The results shown in Fig. 6 with AO on and AO off are relative to the application of the same time varying aberrations. On the other hand, Fig. 6 and movies in Fig. 7–9 report the rms deviation from reference for the 6x6, 10x10 and 15x15 actuators layout. Experimental results show that the average rms deviation from reference passes from 68nm to 28nm for the 15x15, from 58nm to 29nm for the 10x10 and from 53nm to 32nm for the 6x6 for AO Off to AO On. These preliminary results underline the fact that the high resolution wavefront control is more effective in AO correction and demonstrate the flexibility of the system to modify the actuator geometry programmatically via the LCD geometry.

#158841 - $15.00 USD Received 1 Dec 2011; revised 13 Feb 2012; accepted 13 Feb 2012; published 16 Feb 2012

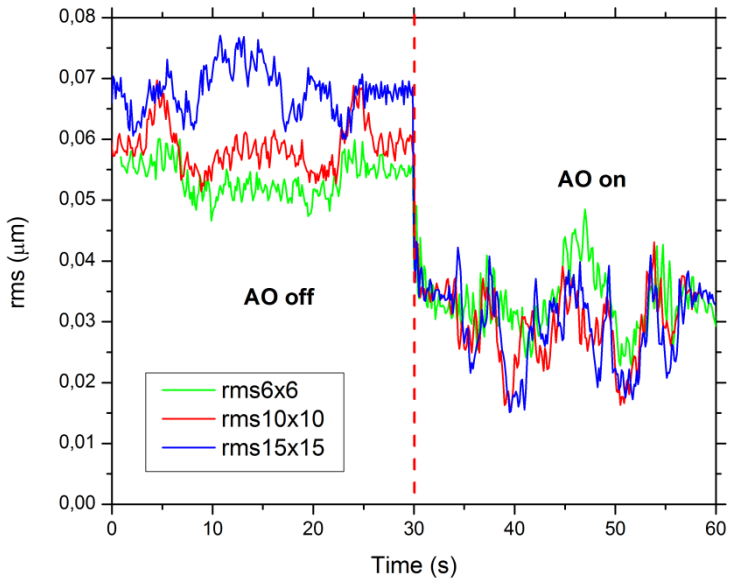

Fig. 6. Rms deviation from reference with the closed loop off and on for the 6x6, 10x10 and 15x15 actuators pattern. The phase screen was moved in and out by 5mm in order to correct for the same aberrations in both conditions.

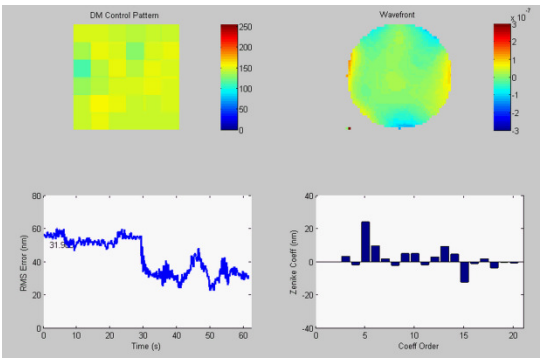

Fig. 7. Adaptive optics closed loop working for the case of the 6x6actuators layout (Media 1).

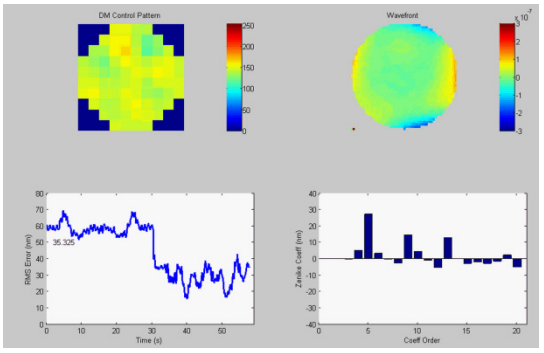

Fig. 8. Adaptive optics closed loop working for the case of the 10x10actuators layout (Media 2).

#158841 - $15.00 USD Received 1 Dec 2011; revised 13 Feb 2012; accepted 13 Feb 2012; published 16 Feb 2012

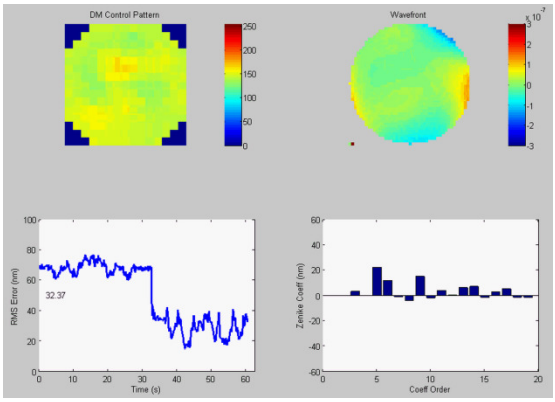

Fig. 9. Adaptive optics closed loop working for the case of the 15x15 actuators layout (Media 3).

5. Zernike Polynomials generation

We also tested the PCDM performances in relation to the Zernike polynomials wavefront forming ability of the mirror. In this series of measurements the wavefront reference programmed to the AO controller was offset with a series of Zernike terms for aberration terms from Z3 to Z20 (according to OSA convention [24]), causing the controller to drive the mirror in best effort at generating the term in question. The performance was then assessed one term at a time by assessing the maximum rms amplitude (for positive and negative offsets) that the mirror could generate before saturating the control output to the mirror. In the particular set of measurement a 10x10 actuator geometry was employed. The results are shown in Fig. 10 where the left hand portion shows the spatial structure of the Zernike terms measured on the system wavefront sensor relative to optical flat together with the control values driving the mirror in each case. As shown, the spatial structure of the modes generated by the mirror are in good keeping with the target terms. In some cases the fitting was limited by the dynamics of the wavefront sensor (ie lenslet focal length) which should be sensitive enough for measuring the influence functions and large enough to support its use with large aberrations.

In the first row the measured polynomials are shown, while the bottom row shows the LCD pattern which has generated them. The PV (peak to valley) amplitude of the surfaces generated before control saturation is shown in the bar chart, in the right hand portion of the diagram compared to the rms error.

#158841 - $15.00 USD Received 1 Dec 2011; revised 13 Feb 2012; accepted 13 Feb 2012; published 16 Feb 2012

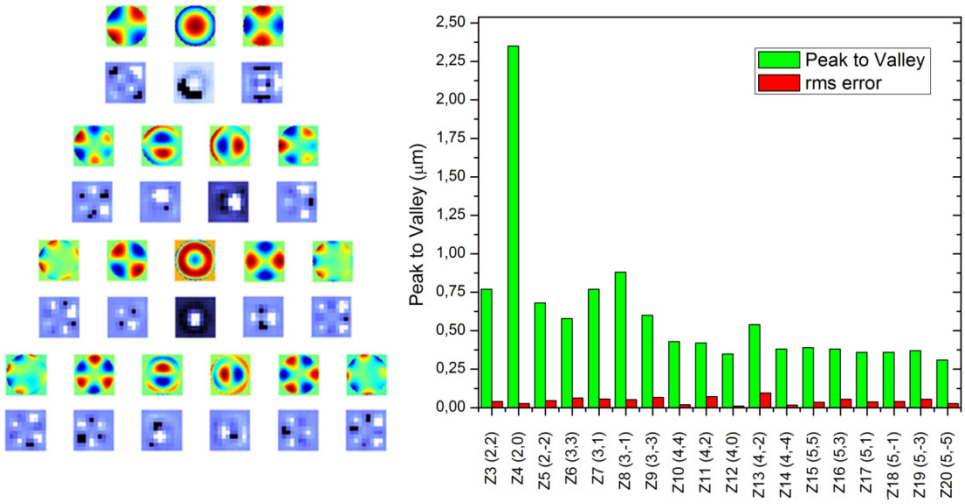

Fig. 10. Left Panel: Zernike polynomials generated by using the closed loop and the patterns necessary for generating them. Right panel: peak to valley amplitude of each Zernike term obtained by the closed loop.

6. High resolution beam manipulation

As a last test, we addressed the capability of high resolution modulation of the PCDM by investigating the intensity modulation at a distance of 2m and by exploiting the full 800x600pixels LCD resolution. As shown qualitatively in Fig. 11, thanks to the high resolution membrane shape control, we have been able to generate alphabet letters by local focusing on the back side of the PCDM.

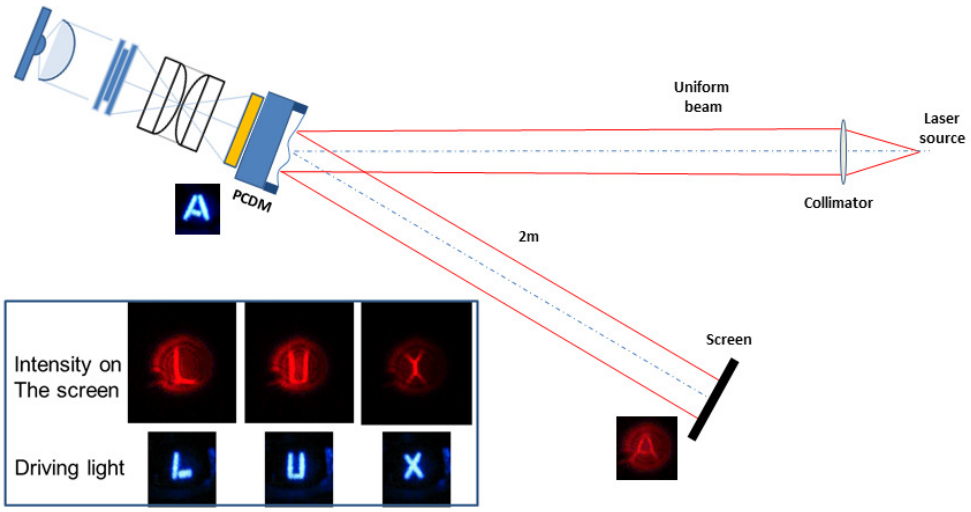

Fig. 11. high resolution control of the light reflected by the PCDM via high resolution addressing of the LCD. The letters of the Latin word for LUX were projected on the back of the PCDM, which resulted in their formation on a screen placed at 2m distance.

#158841 - $15.00 USD Received 1 Dec 2011; revised 13 Feb 2012; accepted 13 Feb 2012; published 16 Feb 2012

7. Conclusions

We have demonstrated that light control of a deformable mirror presents many advantages with respect to the conventional discrete actuators DM, particularly with regards to high resolution wavefront forming systems.

The possibility of controlling the DM shape with high resolution geometries defined in software provides a new level of flexibility in wavefront forming control. With our device it is easy to programmatically address high resolution control geometries, as demonstrated in the 10x10 and 15x15 actuator geometries tested. In the study, the AO correction performance of the mirror for these geometries were compared with that of a 6x6 actuators pattern (which is almost equivalent to the state of the art DM with a size in the range of 10-20mm diameter). The results from our adaptive optics demonstrator highlights that these higher resolution geometries are effective in the reduction of the rms error in closed loop control as well as in the improving the Zernike wavefront forming ability of the system. A significant advantage in the new approach is the absence of cabling problems. The actuator density can be scaled readily to quite dense geometries without modification of the controller and avoiding the usual issue of cabling and control electronics bulk. This paves the way to the realization of larger prototypes for specific applications requiring extremely high resolution, such as astronomy. The extension of this technique to different type of actuators, such as piezo and voice coil, is under investigation.

Acknowledgments

We are grateful to the Science Foundation of Ireland for support under the Grant No. 07/IN.1/I906 and to the National Council of Research of Italy for the Short Term Mobility grant 2011.

#158841 - $15.00 USD Received 1 Dec 2011; revised 13 Feb 2012; accepted 13 Feb 2012; published 16 Feb 2012